Calculations of the $np \rightarrow d\gamma$ reaction in chiral effective field theory

Weijie Du [1,*] Soham Pal,[1] Mamoon Sharaf [1] Peng Yin [1,2] Shiplu Sarker [1] Andrey M. Shirokov [3] and James P. Vary [1]

[1]*Department of Physics and Astronomy, Iowa State University, Ames, Iowa 50010, USA*
[2]*Institute of Modern Physics, Chinese Academy of Sciences, Lanzhou 730000, China*
[3]*Skobeltsyn Institute of Nuclear Physics, Lomonosov Moscow State University, Moscow 119991, Russia*

We present a calculation of the radiative capture cross section of the $np \rightarrow d\gamma$ reaction in the low-energy range, where the $M1$ reaction channel dominates. Employing the LENPIC nucleon-nucleon interaction up to the fifth order (N4LO) that is regularized by the semilocal coordinate space regulators, we obtain the initial and final state wave functions, and evaluate the phase shifts of the scattering state and deuteron properties. We derive the transition operator from the chiral effective field theory up to the next-to-next-to leading order (N2LO), where we also regularize the transition operator using regulators consistent with those of the interactions. We compute the capture cross sections, and the results show a converging pattern with the chiral-order expansion of the nucleon-nucleon interaction, where the regulator dependence of the results is weak when higher-order nucleon-nucleon interactions are employed. We quantify the uncertainties of the cross-section results due to the chiral-order truncation. The chirally complete and consistent cross-section results are calculated up to N2LO and they compare well with the experiments and other theoretical predictions.

I. INTRODUCTION

Nuclear physics plays a fundamental role in studying the evolution of the universe [1,2]. Nuclear astrophysics is nowadays an open field and requires accurate input from nuclear physics [3,4]. However, direct measurements of the cross sections at stellar energies are challenging as many relevant cross sections occur in the experimentally challenging low-energy range [1,2]. It is thus important to develop advanced experimental techniques [5]. Meanwhile, it is equally important to develop first-principles microscopic theories with predictive power.

A promising theoretical approach is the chiral effective field theory (χEFT) [6–8] in combination with model-independent *ab initio* few- and many-body methods (see Ref. [9] and references therein). The χEFT describes the nuclear interactions [10–14] based on the underlying fundamental theory (quantum chromodynamics). It is also employed to derive single-, two-, and multinucleon electroweak currents [15–26]. The model-independent *ab initio* methods utilize direct input from the χEFT, where the consistent scheme of the power expansion for both the nuclear interactions and the nucleon currents enables systematic and quantified convergence study and uncertainty analysis of the calculations [9,12–14].

In this prototypical study, we aim to perform first-principles calculations for nuclear reactions in the energy range of astrophysical interest. For the purpose of demonstration, we study the radiative capture process $np \rightarrow d\gamma$, which

is one of the simplest reactions, yet plays a critical role in big bang nucleosynthesis [1,27,28]. The experimental data for this reaction is sparse in the low energy range [29–32]. Therefore, theoretical studies with predictive power are especially needed.

Indeed, various predictive methods have been developed for precision calculations of the reaction $np \rightarrow d\gamma$ based on either the pionless effective field theory [33–37] or the pionful χEFT [19,38] as alternatives to traditional approaches based on phenomenological models for the nuclear interactions and currents [39–41]. In view of these successful advances, it becomes important to explore new *ab initio* approaches to reaction calculations based on the no-core shell model (NCSM) [42–44] in addition to those already developed, such as the NCSM/RGM approach combining the NCSM with the resonating group method [45–48], and the NCSM with continuum [49–57]. There is also the SS-HORSE-NCSM approach [58–63] that extends the NCSM for studying resonances. We are planning to generalize this approach to *ab initio* calculations of many-body nuclear states in the continuum, not only in the vicinity of resonances, by utilizing the complete harmonic oscillator representation of scattering equations (HORSE) formalism [64]. As the first step, we use here the HORSE approach to calculate continuum states in a simple two-nucleon system.

In this work, we focus on the low-energy range of $np \rightarrow d\gamma$ radiative capture where the $M1$ transition channel dominates. We construct the Hamiltonian matrices for the initial and final nuclear systems using the Low Energy Nuclear Physics International Collaboration (LENPIC) NN interactions [13,14] that are derived from χEFT. We compute the bound and scattering state wave functions via the direct matrix

diagonalization and the HORSE method [64], respectively. We also develop the chiral $M1$ transition operators [16,24,25] with the same semilocal coordinate space (SCS) regulators as those adopted for the LENPIC NN interaction. We perform calculations of the capture cross section and quantify the uncertainty of the results due to the order-by-order truncation of the NN interaction. Chirally consistent and complete calculations are achieved up to the next-to-next-to leading order (N2LO). Our work complements the work by Piarulli *et al.* [19] and that by Acharya and Bacca [38]. However, the differences in the microscopic approaches, the input NN interactions, the choice of regulator schemes, and the systematic convergence and uncertainty analyses distinguish our work.

In Sec. II, we present the elements of the theory, which include the details of computing the initial and final state wave functions, our transition operators, and the cross section. In Sec. III, we show the results of the observables of the deuteron (final state), the phase shifts of the scattering waves (initial state), and the capture cross sections. We conclude in Sec. IV, where we also provide an outlook.

II. THEORY

In this work, we compute the radiative capture cross section of the $np \rightarrow d\gamma$ reaction at low center-of-mass (CM) bombarding energy ($\leqslant 0.01$ MeV) in the relative coordinates of the neutron-proton (np) system. The $M1$ reaction dominates [65][1]: the initial (scattering) state of the np system is in the $^1S_0$ channel, while the final (bound) state is in the $^3SD_1$ channel; and a photon is emitted with the excess energy of the nuclear system during the reaction.

The capture cross section can be calculated based on the transition matrix element [65]

$$\mathcal{M}_\lambda(i, f) = \langle \phi_f | \mu_{1\lambda} | \phi_i \rangle, \quad (1)$$

where $\mu_{1\lambda}$ ($\lambda = 0, \pm 1$) denotes the λ component of the $M1$ transition operator $\vec{\mu}$ (rank-1 tensor). $|\phi_i\rangle$ and $|\phi_f\rangle$ denote the initial and final state vectors of the np system, respectively.

Following the discussion in Ref. [65], we start with the scattering setup where both projections of the total angular momenta of $|\phi_i\rangle$ and $|\phi_f\rangle$ are zeros, without loss of generality.[2] In this case, only the $\lambda = 0$ component of the $M1$ transition operator contributes. The transition probability can be written as [65]

$$T_M(i, f) = \frac{16\pi}{9}\kappa^3 |\mathcal{M}_0(i, f)|^2, \quad (2)$$

---

[1]The contribution from the competing electric dipole $E1$ reaction channel increases with energy. However, even at the highest CM bombarding energy examined here (0.01 MeV), the contribution from the $E1$ reaction channel is about 1% of the total capture cross section [34].

[2]One notes that this transition probability is the same as those computed with the other two choices of the final state polarization, i.e., the projection of the total angular momentum of $|\phi_f\rangle$ being $+1$ (-1), where compatible transition operator μ_{1-1} (μ_{1+1}) should be adopted. This can be seen by applying the Wigner-Eckart theorem [66] to Eq. (1).

where κ is the wave number of the emitted photon. We adopt the natural units and set $\hbar = c = 1$ in this work.

Since there are three possible transitions from the $^1S_0$ state to the deuteron state (with different polarizations) and these transitions are of equal probability, the total $M1$ radiative capture cross section for the unpolarized np system to form a deuteron can be calculated as [65]

$$\sigma = \frac{3}{4\Phi}T_M(i, f), \quad (3)$$

where one sums over the possible polarizations of the final state and averages over the initial polarizations of the np system. Φ denotes the flux of the scattering wave.

In the remainder of this section we describe the methods for solving the Schrödinger equation and calculating the initial and final state wave functions of the reaction. We also derive the $M1$ transition operator based on the χEFT. Though the current work focuses on the two-body reaction problem, our methodology can be generalized to study similar reactions using wave functions from *ab initio* many-body NCSM calculations [42–44,58–63].

A. Nuclear Hamiltonian and basis representation

The Hamiltonian of the np system in relative coordinates is

$$H = T_{\text{rel}} + V_{\text{NN}}, \quad (4)$$

where T_{rel} denotes the relative (intrinsic) kinetic energy and V_{NN} the internucleon interaction.

We employ the three-dimensional harmonic oscillator (3DHO) basis to construct the matrix representation of the Hamiltonian and various operators throughout this work. The wave functions are expanded in a series of 3DHO basis functions that is useful for a straightforward generalization of our approach to studies of many-body nuclear systems within NCSM [42–44] or other *ab initio* approaches.

The 3DHO basis functions of relative motion are specified as $|nlSJM_J\rangle$, where n is the radial quantum number, l is the orbital angular momentum, and S is the total spin of the np system. The total angular momentum J is coupled from l and S, whereas M_J denotes the projection of J. The oscillator quanta is $2n + l$, which is an index to scale the basis dimension. We remark that S, J, M_J and the parity $P_\pi = (-1)^l$ are the good quantum numbers specifying the np system.

In the coordinate representation, the 3DHO basis reads

$$\langle \vec{r}|nlSJM_J\rangle = R_{nl}(r)\sum_{m_l,m_s}(lm_lSm_s|JM_J)Y_{lm_l}(\Omega_{\hat{r}})\chi_{Sm_s}, \quad (5)$$

where the summations over m_l and m_s run over all the possible values of the projections of l and S, respectively. $(lm_lSm_s|JM_J)$ denotes the Clebsch-Gordan coefficient and $Y_{lm_l}(\Omega_{\hat{r}})$ is the spherical harmonics (we adopt the Condon–Shortly convention [66] in this work). χ_{Sm_s} is the spin part of the wave function. The radial part of the oscillator functions is

$$R_{nl}(r) = \sqrt{\frac{2n!}{r_0^3\Gamma(n + l + \frac{3}{2})}}\left(\frac{r}{r_0}\right)^l e^{-\frac{r^2}{2r_0^2}}L_n^{l+\frac{1}{2}}\left(\frac{r^2}{r_0^2}\right) \quad (6)$$

with $L_n^{l+\frac{1}{2}}(r^2/r_0^2)$ and $\Gamma(n + l + 3/2)$ being respectively the associated Laguerre polynomial and the gamma function [67]. The characteristic length scale of the 3DHO basis can be expressed as $r_0 = (\widetilde{m}_N \omega)^{-1/2}$, where ω denotes the oscillator energy and $\widetilde{m}_N$ is the reduced mass of the neutron and proton (set to be 469.46 MeV in this work).

B. The initial state

For our application to very low incident energy, we restrict our discussion of the np scattering to the uncoupled channel that is specified by the quantum numbers l, S, J, and M_J. We calculate the initial state of the np system via the HORSE method [64,68–70]. Based on Eq. (1) in Ref. [64] (where the spin-part of the scattering wave function is ignored), we construct the incoming scattering wave function using the partial wave expansion and couple the orbital angular momentum to the spin of the np system. Taking the relative momentum of the initial np system $\vec{k}$ to be along the $\hat{z}$ axis, the scattering wave function in the uncoupled channel is

$$\langle\vec{r}|\phi_i(\vec{k})\rangle = \frac{1}{k}\sum_{n=0}^{\infty}\sqrt{4\pi(2l+1)}\,a_{nl}(k)R_{nl}(r)$$
$$\times \sum_{m_s}(l0Sm_s|JM_J)Y_{l0}(\theta,\varphi)\chi_{Sm_s}, \qquad (7)$$

where $\vec{r}$ determines the relative position of the nucleons with $r = |\vec{r}|$ and $k = |\vec{k}|$. The polar angle θ is defined as $\cos\theta = \vec{k} \cdot \vec{r}/(kr)$. φ denotes the azimuthal angle. The amplitudes of

the 3DHO basis expansion of the wave function are $\{a_{nl}(k)\}$. We normalize the scattering wave function such that the flux Φ associated with the scattering wave is unity.

The scattering state of the np system satisfies the Schrödinger equation

$$H|\phi_i(\vec{k})\rangle = E|\phi_i(\vec{k})\rangle, \qquad (8)$$

where $E = k^2/(2\widetilde{m}_N)$ is the energy in the CM frame. In the 3DHO basis, the Schrödinger equation is equivalent to the following set of the algebraic equations

$$\sum_{n'=0}^{\infty}\langle nlSJM_J|H - E\delta_{nn'}|n'lSJM_J\rangle\langle n'lSJM_J|\phi_i(\vec{k})\rangle = 0, \quad (9)$$

from which we can obtain the amplitudes $a_{nl}(k) = \langle nlSJM_J|\phi_i(\vec{k})\rangle$ for given values of l, S, J, and M_J.

The HORSE method solves Eq. (9) for the amplitudes $a_{nl}(k)$ by truncating the interaction matrix element $\langle nlSJM_J|V_{NN}|n'lSJM_J\rangle$ in the Hamiltonian up to some large but finite dimension. In particular, one notes that the interaction matrix element decreases with increasing n and n', while the matrix element of the kinetic energy increases linearly with n and $n' \to \infty$ [58,64]. Therefore, a cutoff scale $\widetilde{n}$ is introduced to the interaction matrix in the Hamiltonian of the initial np system; this cutoff scale corresponds to the "boundary" oscillator quanta $\widetilde{N} = 2\widetilde{n} + l$ of the 3DHO basis, which divides the Hamiltonian matrix of the np system into the "interior" region (with interaction) and the complementary "asymptotic" region (free of interaction) as

$$\langle nlSJM_J|H|n'lSJM_J\rangle = \begin{cases} \langle nlSJM_J|T_{\text{rel}} + V_{NN}|n'lSJM_J\rangle & \text{for } n \leqslant \widetilde{n} \text{ and } n' \leqslant \widetilde{n}, \\ \langle nlSJM_J|T_{\text{rel}}|n'lSJM_J\rangle & \text{for } n > \widetilde{n} \text{ or } n' > \widetilde{n}. \end{cases} \qquad (10)$$

This is the only assumption of the HORSE method. In order to improve the convergence of the scattering phase shift and radiative capture cross section, we further apply a "smoothing" scheme [71,72] to the interaction matrix element $\langle nlSJM_J|V_{NN}|n'lSJM_J\rangle$ in Eq. (10). In particular, we substitute $\langle nlSJM_J|V_{NN}|n'lSJM_J\rangle$ in Eq. (10) by the "smoothed" interaction interaction matrix element

$$\langle nlSJM_J|\widetilde{V}_{NN}|n'lSJM_J\rangle = \begin{cases} \sigma_{\widetilde{n}}^{n}\langle nlSJM_J|V_{NN}|n'lSJM_J\rangle\sigma_{\widetilde{n}}^{n'} & \text{for } n \leqslant \widetilde{n} \text{ and } n' \leqslant \widetilde{n}, \\ 0 & \text{for } n > \widetilde{n} \text{ or } n' > \widetilde{n}, \end{cases} \qquad (11)$$

where the smoothing function takes the form [71]

$$\sigma_{\widetilde{n}}^{n} = \frac{1 - e^{-\left[\alpha\frac{n-(\widetilde{n}+1)}{\widetilde{n}+1}\right]^2}}{1 - e^{-\alpha^2}}, \qquad (12)$$

with α being the dimensionless parameter. One can readily check that $\sigma_{\widetilde{n}}^{n}$ has no effect for limited $\widetilde{n}$ when $\alpha \to 0$ or $\alpha \to \infty$. In practice, one takes $\alpha \in [5, 10]$ in order to optimize convergence. In this work, we take $\alpha = 7.5$, and the insensitivity of the phase shift and the capture cross section to $\alpha \in [5, 10]$ was confirmed up through at least the fifth significant digit.

With the truncation of the interaction matrix elements, the amplitudes $\{a_{nl}(k)\}$ are also sorted into two corresponding sets, $\{a_{nl}^{\text{int}}(k)\}$ $(n \leqslant \widetilde{n})$ and $\{a_{nl}^{\text{as}}(k)\}$ $(n > \widetilde{n})$, which are solved as follows. In the asymptotic region, the Hamiltonian is just the kinetic energy operator, which has the tridiagonal matrix form in the 3DHO representation. The amplitudes of the wave function $\{a_{nl}^{\text{as}}(k)\}$ $(n > \widetilde{n})$ obey the three-term recurrence relation

$$\langle nlSJM_J|T_{\text{rel}}|(n-1)lSJM_J\rangle a_{(n-1)l}^{\text{as}}(k) + \langle nlSJM_J|T_{\text{rel}} - E|nlSJM_J\rangle a_{nl}^{\text{as}}(k) + \langle nlSJM_J|T_{\text{rel}}|(n+1)lSJM_J\rangle a_{(n+1)l}^{\text{as}}(k) = 0, \quad (13)$$

where the matrix elements of the kinetic energy operator are

$$\langle(n+1)lSJM_J|T_{\text{rel}}|nlSJM_J\rangle = \frac{1}{2}\omega\sqrt{\left(n + l + \frac{3}{2}\right)(n+1)}, \qquad (14)$$

$$\langle nlSJM_J|T_{\rm rel}|nlSJM_J\rangle = \frac{1}{2}\omega\left(2n + l + \frac{3}{2}\right), \tag{15}$$

$$\langle nlSJM_J|T_{\rm rel}|(n+1)lSJM_J\rangle = \frac{1}{2}\omega\sqrt{\left(n + l + \frac{3}{2}\right)(n+1)}. \tag{16}$$

We adopt two linearly independent solutions for Eq. (13) (see, e.g., Refs. [64,68–70]):

$$S_{nl}(k) = (-1)^n\sqrt{\frac{\pi r_0 n!}{v\Gamma\left(n + l + \frac{3}{2}\right)}}(kr_0)^{l+1}\exp\left(-\frac{k^2 r_0^2}{2}\right)L_n^{l+\frac{1}{2}}\left(k^2 r_0^2\right), \tag{17}$$

$$C_{nl}(k) = \frac{(-1)^{n+l}}{\Gamma\left(-l + \frac{1}{2}\right)}\sqrt{\frac{\pi r_0 n!}{v\Gamma\left(n + l + \frac{3}{2}\right)}}(kr_0)^{-l}\exp\left(-\frac{k^2 r_0^2}{2}\right){}_1F_1\left(-n - l - \frac{1}{2}; -l + \frac{1}{2}; k^2 r_0^2\right), \tag{18}$$

where ${}_1F_1(c; d; x)$ is the confluent hypergeometric function [67].

The asymptotic amplitudes can be expressed as a linear combination of $S_{nl}(k)$ and $C_{nl}(k)$,

$$a_{nl}^{\rm as}(k) = \cos\delta_l S_{nl}(k) + \sin\delta_l C_{nl}(k), \tag{19}$$

where δ_l denotes the scattering phase shift of the partial wave with the orbital angular momentum l. According to Eq. (13), one notes that the above solution holds also for the case when $n = \widetilde{n}$. This will serve as the condition to match the amplitudes in the interior region with those in the asymptotic region.

The amplitudes $\{a_{nl}^{\rm int}(k)\}$ (with $0 \leqslant n \leqslant \widetilde{n}$) in the interior region satisfy the algebraic equation as

$$\sum_{n'=0}^{\widetilde{n}}[\langle nlSJM_J|H|n'lSJM_J\rangle - \delta_{nn'}E]a_{n'l}^{\rm int}(k) = -\delta_{n\widetilde{n}}\langle\widetilde{n}lSJM_J|T_{\rm rel}|(\widetilde{n}+1)lSJM_J\rangle a_{(\widetilde{n}+1)l}^{\rm as}(k). \tag{20}$$

Each amplitude $a_{nl}^{\rm int}(k)$ can be expressed in terms of $a_{(\widetilde{n}+1)l}^{\rm as}(k)$ as [64]

$$a_{nl}^{\rm int}(k) = \mathcal{G}_{n\widetilde{n}}a_{\widetilde{n}+1,l}^{\rm as}(k), \tag{21}$$

with the matrix elements being

$$\mathcal{G}_{nn'} = -\sum_{\nu=0}^{\widetilde{n}}\frac{\langle nlSJM_J|\nu\rangle\langle\nu|n'lSJM_J\rangle}{E_\nu - E}\langle n'lSJM_J|T_{\rm rel}|(n'+1)lSJM_J\rangle, \tag{22}$$

where E_ν and $\langle nlSJM_J|\nu\rangle$ are respectively the eigenvalue and the components of the corresponding eigenvector of the Hamiltonian in the interior region:

$$\sum_{n'=0}^{\widetilde{n}}\langle nlSJM_J|H|n'lSJM_J\rangle\langle n'lSJM_J|\nu\rangle = E_\nu\langle nlSJM_J|\nu\rangle, \quad 0 \leqslant n \leqslant \widetilde{n}. \tag{23}$$

The phase shift δ_l is obtained from the matching condition of the amplitudes (21). In particular, one notes that the amplitude $a_{nl}^{\rm int}(k)$ satisfies Eq. (13) when $n = \widetilde{n} + 1$ and thus both $a_{\widetilde{n}l}^{\rm int}(k)$ and $a_{\widetilde{n}+1,l}^{\rm as}(k)$ can be expressed according to Eq. (19). Therefore, using Eq. (21) the phase shift can be expressed as [64]

$$\tan\delta_l = -\frac{S_{\widetilde{n}l}(k) - \mathcal{G}_{\widetilde{n}\widetilde{n}}S_{\widetilde{n}+1,l}(k)}{C_{\widetilde{n}l}(k) - \mathcal{G}_{\widetilde{n}\widetilde{n}}C_{\widetilde{n}+1,l}(k)}. \tag{24}$$

After calculating the phase shift δ_l at any positive energy E, we get the respective scattering wave function as an infinite expansion in 3DHO basis functions (7) where at $n \geqslant \widetilde{n}$ the amplitudes $a_{nl}(k) = a_{nl}^{\rm as}(k)$ are calculated using Eq. (19) and at $n < \widetilde{n}$ the amplitudes $a_{nl}(k) = a_{nl}^{\rm int}(k)$ are calculated using Eq. (21). In our calculations of the matrix elements of the $M1$ transition operator (see Sec. II D), we restrict the sum in n in Eq. (7) by using only the 3DHO terms with oscillator quanta $2n + l \leqslant N_{\rm max}$ and verify that the accepted value of maximal

allowed quanta $N_{\rm max}$ guarantees the convergence of the phase shift δ_l and the $np \to d\gamma$ radiative capture cross section as well as their independence from the 3DHO basis parameter ω. We remark that we use the same value of $N_{\rm max}$ for the scattering wave function truncation as that for the deuteron ground state wave function (see Sec. II C).

As already mentioned, for our very low-energy application here, we have the initial scattering wave function of the np system in the ${}^1S_0$ state, that is we set $l = 0$, $S = 0$, $J = 0$, and $M_J = 0$.

C. The final state

The final state of the np system is a bound state, the deuteron, characterized by the quantum numbers $J = 1$, $S = 1$ and positive parity, that means that the orbital momentum takes values $l = 0, 2$. We construct the deuteron wave function in the coordinate space as a finite expansion in the 3DHO basis

functions with oscillator quanta $2n + l \leqslant N_{\max}$,

$$\langle \vec{r} | \phi_f \rangle = \sum_{l=0,2} \sum_{n=0}^{\frac{1}{2}(N_{\max}-l)} b_{nl} R_{nl}(r)$$
$$\times \sum_{m_l, m_s} (l m_l S m_s | J M_J) Y_{l m_l}(\Omega_{\hat{r}}) \chi_{S m_s}, \qquad (25)$$

where the amplitudes $\{b_{nl}\}$ satisfy a finite set of algebraic equations:

$$\sum_{l'=0,2} \sum_{n'=0}^{\frac{1}{2}(N_{\max}-l')} \langle nlSJM_J | H - E \delta_{nn'} \delta_{ll'} | n'l'SJM_J \rangle b_{n'l'} = 0,$$

$$l = 0, 2; \ n = 0, 1, \ldots, \frac{1}{2}(N_{\max} - l). \qquad (26)$$

The final state wave function is normalized to unity,

$$\sum_{l=0,2} \sum_{n=0}^{\frac{1}{2}(N_{\max}-l)} |b_{nl}|^2 = 1. \qquad (27)$$

We obtain the amplitudes $\{b_{nl}\}$ by a direct diagonalization of the Hamiltonian matrix $\langle nlSJM_J | H | n'l'SJM_J \rangle$. The truncation boundary $N_{\max}$ is chosen to be large enough and verified to provide convergence and independence from the basis parameter ω of the deuteron binding energy and other observables as well as the calculated cross section of the $np \rightarrow d\gamma$ reaction.

The Hamiltonian of the np system is degenerate in the M_J values. According to the discussion in the beginning of Sec. II, we select $M_J = 0$ for the final state and compute the transition probability and the radiative capture cross section according to Eqs. (2) and (3), respectively.

D. Transition operator

The $M1$ transition in a nuclear system is facilitated by the $M1$ operator which is defined as [73]

$$\vec{\mu} = \frac{1}{2} \int d^3\vec{x} \ \vec{x} \times \vec{\vec{j}}(\vec{x}), \qquad (28)$$

where $\vec{\vec{j}}(\vec{x})$ is a nuclear electromagnetic current in coordinate space. Following convention, this operator is multiplied by a factor of $\sqrt{3/4\pi}$ when calculating the $M1$ transition [74]. As we are working with a two-nucleon (2N) system, we use only the operators derived from one-nucleon (1N) and 2N nuclear electromagnetic currents from Refs. [16,24,25], which are derived from the χEFT and are consistent with the LENPIC NN interactions of Refs. [13,14] adopted in this work. The currents in Refs. [16,24,25] are in momentum space. They can be used in Eq. (28) via the Fourier transformation

$$\vec{\vec{j}}(\vec{x}) = \int \frac{d^3\vec{k}}{(2\pi)^3} e^{i\vec{k}\cdot\vec{x}} \vec{j}(\vec{k}), \qquad (29)$$

where $\vec{j}(\vec{k})$ is the momentum space current. The nuclear electromagnetic currents derived from χEFT are systematically arranged according to a power counting scheme:

$$\vec{j}^{a\mathrm{N}} = \vec{j}_{\mathrm{LO}}^{a\mathrm{N}} + \vec{j}_{\mathrm{NLO}}^{a\mathrm{N}} + \vec{j}_{\mathrm{N2LO}}^{a\mathrm{N}} + \cdots, \qquad (30)$$

where the superscript aN indicates an a-nucleon current (we take $a = 1$ or 2 for the two-nucleon system). It is also worth noting that not all of the orders are present for a particular a-nucleon current.

In this work, we consider only the nuclear electromagnetic currents up to N2LO in the χEFT power counting [16,24,25]. At LO, there is no contribution to the nuclear electromagnetic currents. At NLO, there are both 1N and 2N electromagnetic current operators. In particular, the 1N electromagnetic current operator at NLO is

$$\vec{j}_{\mathrm{NLO}}^{1\mathrm{N}} = \frac{|e|}{4m_N}[-i[\vec{q}_j \times \vec{\sigma}_j](\mu_s + \mu_v \tau_{j,z}) + 2\vec{Q}_j(1 + \tau_{j,z})], \qquad (31)$$

where m_N denotes the nucleon mass (taken to be 938.92 MeV) and e denotes the elementary charge. $\mu_s = 0.880$ and $\mu_v = 4.706$ are the isoscalar and isovector anomalous magnetic moments of the nucleus, respectively. $\vec{q}_j = \vec{p}'_j - \vec{p}_j$, $\vec{Q}_j = (\vec{p}'_j + \vec{p}_j)/2$ are the linear combinations of the incoming ($\vec{p}_j$) and outgoing ($\vec{p}'_j$) momenta of the jth nucleon. $\vec{\sigma}_j$ denotes the spin operator of the jth nucleon, while $\vec{\tau}_j$ is the isospin operator of the jth nucleon. The projection of $\vec{\tau}_j$ is $\tau_{j,z}$. Meanwhile, the 2N electromagnetic current operator at NLO is

$$\vec{j}_{\mathrm{NLO}}^{2\mathrm{N}} = \frac{i|e|g_A^2}{4F_\pi^2}[\vec{\tau}_j \times \vec{\tau}_k]_z \frac{\vec{\sigma}_k \cdot \vec{q}_k}{q_k^2 + m_\pi^2}\left(\vec{q}_j \frac{\vec{\sigma}_j \cdot \vec{q}_j}{q_j^2 + m_\pi^2} - \vec{\sigma}_j\right)$$
$$+ (j \leftrightharpoons k), \qquad (32)$$

where $(j \leftrightharpoons k)$ indicates the term with swapped nucleon indices $j = 1, 2$ and $k = 1, 2$ (and $j \neq k$) for the two-nucleon system. $g_A = 1.29$ denotes the axial coupling constant, $F_\pi = 92.4$ MeV is the pion decay constant, $m_\pi = 138.03$ MeV is the average pion mass.

At N2LO, there is a 1N current operator

$$\vec{j}_{\mathrm{N2LO}}^{1\mathrm{N}} = -\frac{i|e|g_A^2 \tau_{j,z}}{32\pi F_\pi^2}[m_\pi - (4m_\pi^2 + q_j^2)A(|\vec{q}_j|)][\vec{q}_j \times \vec{\sigma}_j], \qquad (33)$$

where $A(q) = \frac{1}{2q} \tan^{-1}(\frac{q}{m_\pi})$. At this order, there is no 2N current operator.

In this work we have used a version of the LENPIC NN interactions described in [13,14]. These potentials have been regularized in coordinate space by multiplying them with the following coordinate space function:

$$f\left(\frac{r}{R}\right) = \left[1 - \exp\left(-\frac{r^2}{R^2}\right)\right]^6, \qquad (34)$$

where R is the regulator parameter. In this work we take $R = 0.9$ and 1.0 fm. Note that only the V_{NN} are regularized by $f(r/R)$, while the T_{rel} is not regularized. Thus for consistency we also regularize the 2N current operator in Eq. (32), but not the 1N current operator [in Eqs. (31) and (33)], by multiplying it with this same function $f(r/R)$. Consistency can be proved based on the continuity equation of the nuclear charge and current operators.

We can derive the contributions from $\vec{j}_{\mathrm{NLO}}^{1\mathrm{N}}$, $\vec{j}_{\mathrm{NLO}}^{2\mathrm{N}}$, and $\vec{j}_{\mathrm{N2LO}}^{1\mathrm{N}}$ to the $M1$ transition operator $\vec{\mu}$ according to Eqs. (28)

TABLE I. Deuteron properties computed with the χEFT LENPIC NN interactions up to N4LO with the SCS regulator $R = 0.9$ fm (B) and $R = 1.0$ fm (C): the ground state energy E_{gs}, the point-proton rms r_d, the magnetic dipole moment μ_D, the electric quadrupole moment Q, and the d-wave probability P_d. The theoretical predictions obtained with LENPIC N4LO interactions in Refs. [13,77], together with other empirical results [78–82], are also provided for comparison.

R (fm)	χ order	E_{gs} (MeV)	r_d (fm)	μ_D (μ_N)	Q ($e\,\mathrm{fm}^2$)	P_d (%)
B	LO	−2.023 47	1.989 75	0.865 311	0.229 983	2.5440
	NLO	−2.198 67	1.968 28	0.852 837	0.273 398	4.7335
	N2LO	−2.231 08	1.965 51	0.854 154	0.270 359	4.5025
	N3LO	−2.223 25	1.972 21	0.855 946	0.270 648	4.1878
	N4LO	−2.223 25	1.971 31	0.855 388	0.270 985	4.2858
C	LO	−2.083 46	1.978 90	0.868 564	0.214 659	1.9731
	NLO	−2.206 09	1.966 62	0.855 659	0.271 370	4.2383
	N2LO	−2.235 16	1.964 36	0.856 323	0.269 874	4.1217
	N3LO	−2.223 26	1.975 35	0.852 620	0.274 565	4.7717
	N4LO	−2.223 26	1.974 31	0.854 718	0.272 428	4.4034
LENPIC-B [13]	N4LO	−2.2246	1.972		0.271	4.29
LENPIC-B [77]	N4LO	−2.2233[a]				
LENPIC-C [77]	N4LO	−2.2233	1.9743	0.8547	0.2724	4.4034
Empirical		−2.224 575(9) [78]	1.975 35(85) [79]	0.857 438 231 1(48) [80]	0.2860(15) [81,82]	

[a]As suggested in Ref. [77], relativistic corrections are necessary in order to compare with −2.2246 MeV in Ref. [13].

and (29). In particular, for the 2N system, we have[3]

$$\vec{\mu}_{\mathrm{NLO}}^{1\mathrm{N}} = \frac{1}{2}[(\mu_s + \mu_v \tau_{j,z})\vec{\sigma}_j + (1 + \tau_{j,z})\vec{l}_j] + (j \leftrightharpoons k), \quad (35)$$

$$\vec{\mu}_{\mathrm{NLO}}^{2\mathrm{N}} = -\frac{g_A^2 m_N m_\pi}{16\pi F_\pi^2}[\vec{\tau}_j \times \vec{\tau}_k]_z[(1 + m_\pi r)([\vec{\sigma}_j \times \vec{\sigma}_k] \cdot \hat{r})\hat{r}$$
$$- m_\pi r[\vec{\sigma}_j \times \vec{\sigma}_k]]\frac{e^{-m_\pi r}}{m_\pi r}, \quad (36)$$

$$\vec{\mu}_{\mathrm{N2LO}}^{1\mathrm{N}} = 0, \quad (37)$$

where the $\vec{\mu}_{\mathrm{NLO}}^{1\mathrm{N}}$, $\vec{\mu}_{\mathrm{NLO}}^{2\mathrm{N}}$, and $\vec{\mu}_{\mathrm{N2LO}}^{1\mathrm{N}}$ operators correspond to the contributions from $\vec{j}_{\mathrm{NLO}}^{1\mathrm{N}}$, $\vec{j}_{\mathrm{NLO}}^{2\mathrm{N}}$, and $\vec{j}_{\mathrm{N2LO}}^{1\mathrm{N}}$, respectively. The unit vector is $\hat{r} = \vec{r}/r$. In obtaining $\vec{\mu}_{\mathrm{NLO}}^{2\mathrm{N}}$ from $\vec{j}_{\mathrm{NLO}}^{2\mathrm{N}}$, we transform the single-particle coordinates to the relative coordinates, while we keep track of the single-particle spinor and isospinor wave functions. The contribution from the CM part of $\vec{j}_{\mathrm{NLO}}^{2\mathrm{N}}$ is suppressed with this transformation [76] for the isolated np system but will be retained in planned calculations for many-nucleon systems.

Thus, we have the $M1$ transition operator up to N2LO as

$$\vec{\mu} = \vec{\mu}_{\mathrm{NLO}}^{1\mathrm{N}} + \vec{\mu}_{\mathrm{NLO}}^{2\mathrm{N}}, \quad (38)$$

where both the 1N operator $\vec{\mu}_{\mathrm{NLO}}^{1\mathrm{N}}$ and the 2N operator $\vec{\mu}_{\mathrm{NLO}}^{2\mathrm{N}}$ appear at NLO according to the power counting scheme in Refs. [16,24,25]. We note that, in the literature, $\vec{\mu}_{\mathrm{NLO}}^{1\mathrm{N}}$ and $\vec{\mu}_{\mathrm{NLO}}^{2\mathrm{N}}$ are also referred to as the impulse approximation (IA) and meson exchange current (MEC) operators, respectively. For practical numerical calculations in this work, we compute the matrix elements of $\vec{\mu}_{\mathrm{NLO}}^{1\mathrm{N}}$ and $\vec{\mu}_{\mathrm{NLO}}^{2\mathrm{N}}$ for the np system

in the 3DHO representation; more details are available in Ref. [75,76].

III. RESULTS AND DISCUSSION

A. Deuteron wave function and observables

We compute the final state (deuteron) wave functions with the LENPIC NN interactions up to N4LO derived with the SCS regulators $R = 0.9$ or 1.0 fm. Based on the deuteron wave functions, we calculate various deuteron properties, which include the ground state energy, the rms point charge radius, the magnetic dipole moment,[4] and the electric quadrupole moment, as well as the d-wave probability. In each of our calculations, a sufficiently large model space is retained for convergence analysis (set to be $N_{\max} = 2000$). While we set $\omega = 28$ MeV in this work, we checked that the converged results are independent of ω over a range of values ($\omega \in [10, 40]$ MeV at least) for this large model space to the quoted significant figures in Table I. Note that there is no Hungarian smoothing adopted for the ground-state calculations throughout the paper.

For each observable and choice of regulator, the expectation value also shows a converging trend as a higher order of the LENPIC NN interactions is employed (the d-wave probability is not an observable): the order-by-order correction of the observable decreases with the chiral order of the NN interaction. For comparison, we also present (1) the reference values computed by the LENPIC group with the NN interactions up to the fifth order (N4LO) [13,77], and (2) respective

---

[3]Interested readers are referred to Refs. [75,76] for detailed derivations.

[4]Here, we make use of the one-nucleon operator only to calculate the magnetic dipole moment. Up to N2LO, there is no two-nucleon current contribution to the magnetic dipole moment of the deuteron (isospin $T = 0$ channel).

TABLE II. Scattering phase shift δ_0 (in degrees) of the np system in the $^1S_0$ channel computed with the χEFT LENPIC NN interactions up to N4LO with the SCS regulator $R = 1.0$ fm for six CM bombarding energies: $E_1 = 1.2625 \times 10^{-8}$ MeV, $E_2 = 5 \times 10^{-7}$ MeV, $E_3 = 5 \times 10^{-4}$ MeV, $E_4 = 1 \times 10^{-3}$ MeV, $E_5 = 5 \times 10^{-3}$ MeV, and $E_6 = 1 \times 10^{-2}$ MeV. The phase shifts obtained based on the LO NN interaction with $R = 0.9$ fm are presented in the parentheses. Our results are quoted to four significant figures while calculations were performed to attain at least five significant figures of precision. The theoretical predictions of the LENPIC collaboration employing the N4LO NN interactions with $R = 1.0$ fm [13,14,77] (denoted as N4LO*) are provided for direct comparisons (corresponding predictions with $R = 0.9$ fm [13,14,77] agree with those with $R = 1.0$ fm and are hence omitted). The phase shift results computed by the effective range expansion (denoted as ERE) are also presented.

χ order	$\delta_0(E_1)$	$\delta_0(E_2)$	$\delta_0(E_3)$	$\delta_0(E_4)$	$\delta_0(E_5)$	$\delta_0(E_6)$
LO	0.021 95 (0.021 52)	0.1381 (0.1354)	4.358 (4.273)	6.149 (6.030)	13.51 (13.26)	18.72 (18.38)
NLO	0.023 73	0.1494	4.711	6.644	14.56	20.09
N2LO	0.023 73	0.1494	4.710	6.644	14.56	20.09
N3LO	0.023 73	0.1494	4.711	6.644	14.56	20.09
N4LO	0.023 73	0.1493	4.709	6.643	14.55	20.09
N4LO*	0.023 72	0.1493	4.708	6.640	14.55	20.08
ERE	0.023 74	0.1494	4.712	6.646	14.56	20.09

empirical values [78–82] in Table I. We find that our results for the observables computed up to N4LO agree well with both independent theoretical results and with the empirical values.

The computed d-wave probabilities P_d in the deuteron are also shown. They should not be interpreted as the order-by-order convergence with the power expansion scheme of the LENPIC NN interactions. We find that these results compare well with the corresponding results from Refs. [13,77] quoted in Table I.

We observe a moderate regulator dependence of all the computed deuteron properties: different choices of the regulator can result in a difference at the third decimal place for most quantities. Exceptions are the ground state energy and the quadrupole moment results obtained with the LO NN interactions, where the difference is at the second decimal place.

B. Scattering wave function and phase shift

We calculate the initial state of the nuclear system at six CM bombarding energies: $E_1 = 1.2625 \times 10^{-8}$ MeV, $E_2 = 5 \times 10^{-7}$ MeV, $E_3 = 5 \times 10^{-4}$ MeV, $E_4 = 1 \times 10^{-3}$ MeV, $E_5 = 5 \times 10^{-3}$ MeV, and $E_6 = 1 \times 10^{-2}$ MeV.[5] Working with the HORSE method, we use a sufficiently large cutoff of the boundary oscillator quanta $\widetilde{N} = 2\widetilde{n} + l$ (taken to be $\widetilde{N} = 180$) for the interaction matrix for the NN interaction in order to obtain the converged phase shift δ_0. We confirmed the convergence of δ_0 with $\widetilde{N}$. We also confirmed that the converged phase shifts are independent of $\widetilde{N}$ for $\widetilde{N} \geqslant 180$ (at least) and of ω for $\omega \in [10, 40]$ MeV (at least) when the smoothed interaction [Eq. (11)] is used.

In Table II, we present the results of the scattering phase shift δ_0 of the initial np system in the $^1S_0$ channel as a function of (1) the LENPIC NN interactions (with the SCS regulator $R = 1.0$ fm), and (2) the bombarding energy E_i

---

[5]The $np \to d\gamma$ capture cross sections at these CM bombarding energies are also calculated in Ref. [34] within pionless effective field theory, except for the case of E_2.

($i = 1, 2, \ldots, 6$). The results based on the LENPIC NN interactions with the SCS regulator $R = 0.9$ fm are not shown as they agree with the results shown in Table II; exceptions are the results based the LO NN interaction (with $R = 0.9$ fm), which are presented in the parentheses for comparison.

Our results based on the LO, NLO, N2LO, N3LO, and N4LO NN interactions employing different SCS regulators (either $R = 0.9$ or 1.0 fm) agree well with the theoretical predictions of LENPIC [13,14,77]. We also note that our results with higher-order NN interactions agree well with those obtained by the effective range expansion (ERE) based on Ref. [83] (with the associated percentage errors evaluated to be less than 0.04% of respective nominal values shown in Table II).

C. Radiative capture cross section

We calculate the radiative capture cross section of the $np \to d\gamma$ reaction at six selected CM bombarding energies E_1, E_2, E_3, E_4, E_5, and E_6. In our calculations, we adopt the consistent SCS regulator ($R = 0.9$ or 1.0 fm) for both the transition operator and the LENPIC NN interaction. In each calculation, the consistent LENPIC NN interaction (i.e., the same chiral order and SCS regulator) is adopted to calculate both the initial and final wave functions, whereas either solely the 1N transition operator or both the 1N and 2N (1N + 2N) transition operators are adopted.

We study the convergence of the capture cross section at each chiral order truncation of the χEFT LENPIC NN interaction with fixed choices of the transition operator (either 1N or 1N + 2N operator). As mentioned above, in calculations of the radiative capture cross section we truncate the expansion of the scattering wave function in the series of 3DHO functions [see Eq. (7)] at the same oscillator quanta $2n + l \leqslant N_{max} = 2000$ as in the deuteron ground state. With a sufficiently large interaction matrix truncated at $\widetilde{N}$ oscillator quanta that ensures the convergence of the phase shift of the scattering wave function, we find that the results of the capture cross section converge with N_{max} to at least five significant figures. We also checked that the converged cross-section

TABLE III. The $np \to d\gamma$ capture cross section (in millibarns) via the $M1$ reaction channel at six CM bombarding energies (see Table II). The theoretical predictions of the capture cross section via the $M1$ channel in Ref. [34] are also shown. The experimental cross sections of Refs. [29,30] and theoretical results of Refs. [37,38] with the CM bombarding energy $E_1 = 1.2625 \times 10^{-8}$ MeV are presented for comparison; these cross sections include also the contributions from the $E1$ reaction channel, which, however, are expected to be several orders of magnitude smaller than those from the $M1$ reaction channel [34]. The bold values are from the chirally consistent/complete calculations up to NLO and N2LO in this work. We quote cross-section uncertainties in parentheses based on a Bayesian analysis of chiral-order truncation of the NN interaction [84]. The one-sigma uncertainty is quoted for the underscored least significant digits of each result. See the text for the discussion of the Bayesian analysis employed and other details.

	χ order	$\sigma(E_1)$	$\sigma(E_2)$	$\sigma(E_3)$	$\sigma(E_4)$	$\sigma(E_5)$	$\sigma(E_6)$
1N	LO	240(100)	38(16)	1.2(5)	0.8(4)	0.36(15)	0.24(10)
	NLO	301(10)	47.9(1.6)	1.50(5)	1.06(3)	0.446(15)	0.30(1)
	N2LO	311(3)	49.4(5)	1.550(15)	1.09(1)	0.460(5)	0.305(3)
	N3LO	307(3)	48.8(5)	1.531(15)	1.07(1)	0.455(4)	0.301(3)
	N4LO	308(3)	48.9(5)	1.535(15)	1.08(1)	0.456(5)	0.302(3)
1N + 2N	LO	247(100)	39(16)	1.2(5)	0.9(4)	0.37(15)	0.25(10)
	NLO	**312(10)**	**49.6(1.6)**	**1.56(5)**	**1.09(3)**	**0.462(15)**	**0.31(1)**
	N2LO	**322(3)**	**51.1(5)**	**1.605(15)**	**1.13(1)**	**0.477(5)**	**0.316(3)**
	N3LO	319(3)	50.6(5)	1.590(15)	1.12(1)	0.472(4)	0.313(3)
	N4LO	319(3)	50.8(5)	1.594(15)	1.12(1)	0.473(5)	0.313(3)
Ref. [34]		334.2		1.667(0)	1.170(0)	0.4950(0)	0.3279(0)
Ref. [37]		334.9($^{+5.2}_{-5.4}$)					
Ref. [38]		321.0(± 0.7)					
Expt. [29]		334.2(± 0.5)					
Expt. [30]		332.6(± 0.7)					

results are independent of $\widetilde{N}$, $N_{\max}$, and the 3DHO basis parameter ω.

We also study the regulator dependence of the converged cross-section results. In particular, we find that the percentage differences between the nominal values of the cross section computed with either $R = 0.9$ fm or $R = 1.0$ fm regulators are (1) <10% with NN interactions up to LO (2) <1% with NN interactions up to NLO (3) <0.6% with NN interactions up to N2LO (4) <0.01% with NN interactions up to N3LO, and (5) <0.5% with NN interactions up to N4LO, when the 1N transition operator is employed [recall that the 1N transition operator receives no pion-current contribution and is not regularized by the regulator Eq. (34)]. The corresponding percentage differences with the $1N + 2N$ transition operator (recall that the 2N part of the transition operator is regularized by the consistent SCS regulator as that of the NN interaction employed) are (1) <9% with LO NN interactions, (2) <0.6% with NN interactions up to NLO, and (3) <0.2% with the NN interactions up to N2LO, N3LO, and N4LO. These differences suggest a weak regulator dependence of the cross-section results computed with higher-order NN interactions.

We find that the capture cross-section results converge with the chiral expansion of the NN interaction for fixed bombarding energy and transition operator (either 1N or $1N + 2N$ operator), while the order-by-order corrections in the results decrease. For fixed choices of the transition operator, the one-sigma uncertainties of the cross-section results are dominated by the chiral-order-truncation uncertainties of the NN interactions; these uncertainties are analyzed in the systematic framework of the Bayesian analysis [84] (see Appendix for

details). We adopt the viewpoint that the chiral-order uncertainty is best determined up to N2LO (where the calculations are chirally consistent with the $1N + 2N$ current) and cannot be improved at higher chiral order due to the limited current we employ. Therefore, we quote chiral uncertainties at chiral orders beyond N2LO to be the same as those at N2LO.

In Table III, we present the cross-section results as functions of the chiral order of LENPIC NN interactions (up to N4LO) and the transition operators (either 1N or $1N + 2N$ current operators up to N2LO), where the SCS regulator regularizing both the NN interactions and the transition operators is taken to be $R = 1.0$ fm. Corresponding one-sigma uncertainties from the Bayesian analysis are also presented. Within the error bars, the cross-section results computed with the SCS regulators $R = 0.9$ fm agree with those obtained with $R = 1.0$ fm. For the purpose of illustration, we also present the plot of the cross-section results (obtained with $R = 1.0$ fm) for the case with the CM bombarding energy E_1 as a function of the chiral order of the LENPIC NN interaction, and the transition operator in Fig. 1. The plots of the results with the other regulator $R = 0.9$ fm and CM bombarding energies are similar.

Based on Table III, we find, in general, that the capture cross section decreases with increasing bombarding energy for fixed NN interaction and transition operator. For all the calculations, our additional 2N transition operator enhances respective cross sections calculated with merely the 1N transition operator by a few percent.

Based on the $1N + 2N$ transition operator (recall this operator is complete up to NLO and there is no contribution to the transition operator at N2LO), we perform chirally
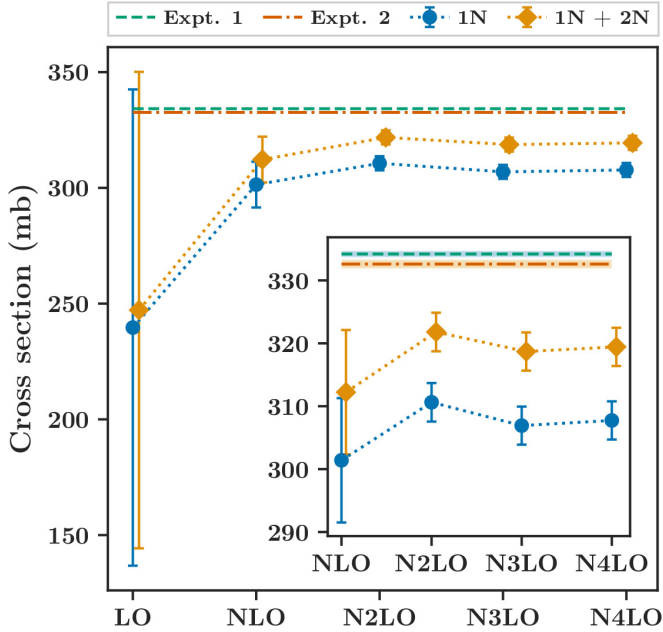
FIG. 1. The $np \to d\gamma$ capture cross section via the $M1$ reaction channel at the CM bombarding energy $E_1 = 1.2625 \times 10^{-8}$ MeV calculated with χEFT LENPIC NN interactions up to N4LO with $R = 1.0$ fm, where either 1N transition operator (blue) or both 1N + 2N transition operators (brown) with $R = 1.0$ fm are employed. The one-sigma error bars for the cross-section results are obtained via Bayesian analysis [84] (see the text for the discussion of the Bayesian analysis employed and other details). The measured cross sections, 334.2($\pm$0.5) mb [29] and 332.6($\pm$0.7) mb [30], are also presented as green and red dashed lines (with the corresponding shaded areas denoting the error bars), respectively.

consistent/complete calculations up to NLO and also to N2LO employing the corresponding NN interactions. These chirally consistent/complete results are highlighted by the bold fonts in Table III, where the results complete up to N2LO compare well with the experiments [29,30], and the theoretical predictions of Refs. [34,37] based on pionless effective field theory via either perturbative or lattice QCD calculations. We remark that our chirally consistent/complete calculation up to N2LO at the bombarding energy E_1 compare well with the prediction in Ref. [38], which is computed with the χEFT potential regularized by the semilocal momentum space regulator [85] and the multipole expansions of the electromagnetic currents derived within χEFT [15,16,86,87]. Our chirally consistent/complete calculation up to N2LO provides an uncertainty of about 1% of the nominal value, which is reasonable when compared with the N3LO chiral uncertainty of 0.2% quoted by Acharya and Bacca [38].

The cross-section results with higher-order (i.e., N3LO and N4LO) NN interactions are also presented in Table III. These results should be regarded as chirally incomplete (as the transition operators are only consistent up to N2LO). More systematic calculations necessitate developing the chirally consistent higher-order transition operators, which are expected to improve the precision and accuracy of our calculations [19,38]; this will be the focus of future work.

IV. SUMMARY AND OUTLOOK

In this work, we focus on the radiative capture of a neutron by a proton $np \to d\gamma$ at very low energies: the bombarding energy in the center-of-mass frame is less or equal to 0.01 MeV, where the $M1$ transition dominates. The input of our calculations, the NN interactions and the transition operators, are from the χEFT [6–8], which is a low-energy theory of quantum chromodynamics.

In particular, we construct the Hamiltonians of the np system using the χEFT LENPIC [12] NN interactions [13,14] up to the N4LO with the semilocal coordinate space regulators $R = 0.9$ or 1.0 fm. The deuteron wave functions are obtained by a direct matrix diagonalization. These wave functions are used to compute the deuteron properties, where the results exhibit a moderate regulator dependence. We find that the computed deuteron observables converge when higher-order LENPIC NN interactions are employed. Our results compare well with those of others [13,77] and with empirical results [78–82].

We compute the scattering wave functions of the initial scattering state in the np system by the HORSE method using the same χEFT LENPIC NN interactions. We find that the phase shift results computed with higher-order NN interactions have negligible regulator dependence and they agree well with those obtained by the effective range expansion [83].

We compute the $M1$ transition operator up to N2LO within the same χEFT framework adopted in developing the NN interactions in this work. The transition operator consists of the one-nucleon (impulse approximation) and two-nucleon (meson exchange current) operators. We regularize the two-body current operator by the consistent semilocal coordinate space regulators utilized in the NN interactions.

Combining the initial and final state wave functions of the np system together with the transition operator, we calculate the $np \to d\gamma$ reaction cross section. We find that the additional two-nucleon operator enhances the cross sections by a few percent in all calculations which improves agreement between theory and experiment where available. The regulator dependence of the cross-section results is weak when higher-order NN interactions are included. Our results converge with the chiral expansion of the NN interactions. The uncertainties of the cross-section results are dominated by the chiral-order truncation of the NN interaction when compared with uncertainties from our numerical methods. We quantify these uncertainties by Bayesian analysis [84].

The chirally consistent/complete calculations of the $np \to d\gamma$ reaction cross section are performed with the consistent NN interactions and transition operator up to N2LO. The results compare well with other theoretical studies [34,37,38] and with experiments [29,30]. The calculations with NN interactions of higher orders are also presented.

Going forward, it will be important to systematically investigate the contributions from the nuclear electromagnetic current operators up to higher chiral orders. This will enable us to perform precision calculations for a wide class of photon-induced nuclear reactions. As *ab initio* microscopic reaction theories provide predictive power in the

investigations of the radiative capture cross section (especially valuable for astrophysics applications at extremely low energies), it will also be important to generalize the current method to study the nucleon capture reactions on other nucleus. Such research will, in turn, provide an important test bed for the on- and off-shell properties of internucleon interactions and insights on the nuclear response to external probes.

APPENDIX: THE BAYESIAN ANALYSIS

Following Ref. [84], we consider a χEFT expansion of a general scattering observable y as a function of a d-dimensional real variable x:

$$y(x) = y^{(0)}(x) + \Delta y^{(2)}(x) + \Delta y^{(3)}(x) + \cdots$$
$$= y_{\text{ref}}(x)[c_0(x) + c_2(x)Q^2 + c_3(x)Q^3 + \cdots], \quad \text{(A1)}$$

where $\Delta y^{(2)}(x) = y^{(2)}(x) - y^{(0)}(x)$ and $\Delta y^{(j)}(x) = y^{(j)}(x) - y^{(j-1)}(x)$ $(j = 3, 4, \ldots)$, with the superscripts denoting the chiral order. Q is the ratio of the soft scale to the hard scale of the χEFT. The dimensionful quantity $y_{\text{ref}}(x)$ sets the overall scale. The dimensionless coefficients $\{c_0(x), c_2(x), c_3(x), \ldots\}$ are assumed to be drawn from an underlying Gaussian Process with a constant mean $\bar{\mu}$, and a squared exponential kernel

$$\kappa(x, x'; \bar{c}, h) = \bar{c}^2 e^{-(x-x')^T (x-x')/(2h)^2}, \quad \text{(A2)}$$

with $\bar{c}$ and h being the parameters. This allows us to get the analytical expressions for the posterior probability distributions of $\{\Delta y^{(0)}(x), \Delta y^{(2)}(x), \Delta y^{(3)}(x), \ldots\}$ (see Ref. [84] for details).

For the application in this work, y is the cross section and x is the bombarding energy. We assume a Gaussian prior for $\bar{\mu}$, and an inverse χ^2 distribution for $\bar{c}$. We take the point estimates $Q = 0.31$ and $h = 0.06$ MeV. The maximum *a posteriori* values of Q and h, that we find after carrying out the Bayesian analysis, are approximately 0.29 and 0.063 MeV, respectively. The agreement with the maximum *a posteriori* Q and h values justifies our choice of the prior Q and h values. Finally, we take y_{ref} to be the cross-section results based on our chirally consistent and complete calculations up to N2LO.

[1] I. J. Thompson and F. M. Nunes, *Nuclear Reactions for Astrophysics: Principles, Calculation and Applications of Low-Energy Reactions*, 1st ed. (Cambridge University Press, Cambridge, 2009).

[2] D. R. Phillips, Annu. Rev. Nucl. Part. Sci. **66**, 421 (2016).

[3] S. Burles, K. M. Nollett, J. W. Truran, and M. S. Turner, Phys. Rev. Lett. **82**, 4176 (1999).

[4] S. Burles, K. M. Nollett, and M. S. Turner, Astrophys. J. Lett. **552**, L1 (2001).

[5] C. Broggini, D. Bemmerer, A. Guglielmetti, and R. Menegazzo, Annu. Rev. Nucl. Part. Sci. **60**, 53 (2010).

[6] S. Weinberg, Nucl. Phys. B **363**, 3 (1991).

[7] S. Weinberg, Phys. Lett. B **251**, 288 (1990).

[8] S. Scherer and M. R. Schindler, *A Primer for Chiral Perturbation Theory* (Springer, Berlin, 2012).

[9] P. Maris, E. Epelbaum, R. J. Furnstahl, J. Golak, K. Hebeler, T. Hüther, H. Kamada, H. Krebs, U.-G. Meißner, J. A. Melendez, A. Nogga, P. Reinert, R. Roth, R. Skibiński, V. Soloviov, K. Topolnicki, J. P. Vary, Y. Volkotrub, H. Witała, and T. Wolfgruber (LENPIC Collaboration), Phys. Rev. C **103**, 054001 (2021).

[10] D. R. Entem and R. Machleidt, Phys. Rev. C **68**, 041001(R) (2003).

[11] R. Machleidt and D. R. Entem, Phys. Rep. **503**, 1 (2011).

[12] E. Epelbaum, H.-W. Hammer, and U.-G. Meißner, Rev. Mod. Phys. **81**, 1773 (2009).

[13] E. Epelbaum, H. Krebs, and U.-G. Meißner, Phys. Rev. Lett. **115**, 122301 (2015).

[14] E. Epelbaum, H. Krebs, and U.-G. Meißner, Eur. Phys. J. A **51**, 53 (2015).

[15] S. Pastore, R. Schiavilla, and J. L. Goity, Phys. Rev. C **78**, 064002 (2008).

[16] S. Kölling, E. Epelbaum, H. Krebs, and U.-G. Meissner, Phys. Rev. C **80**, 045502 (2009).

[17] S. Pastore, L. Girlanda, R. Schiavilla, M. Viviani, and R. B. Wiringa, Phys. Rev. C **80**, 034004 (2009).

[18] S. Pastore, L. Girlanda, R. Schiavilla, and M. Viviani, Phys. Rev. C **84**, 024001 (2011).

[19] M. Piarulli, L. Girlanda, L. E. Marcucci, S. Pastore, R. Schiavilla, and M. Viviani, Phys. Rev. C **87**, 014006 (2013).

[20] R. Schiavilla, A. Baroni, S. Pastore, M. Piarulli, L. Girlanda, A. Kievsky, A. Lovato, L. E. Marcucci, S. C. Pieper, M. Viviani *et al.*, Phys. Rev. C **99**, 034005 (2019).

[21] A. Baroni, R. Schiavilla, L. E. Marcucci, L. Girlanda, A. Kievsky, A. Lovato, S. Pastore, M. Piarulli, S. C. Pieper, M. Viviani *et al.*, Phys. Rev. C **98**, 044003 (2018).

[22] G. B. King, L. Andreoli, S. Pastore, M. Piarulli, R. Schiavilla, R. B. Wiringa, J. Carlson, and S. Gandolfi, Phys. Rev. C **102**, 025501 (2020).

[23] E. Epelbaum, *Proceedings of the International Conference "Nuclear Theory in the Supercomputing Era–2018" (NTSE-2018), Daejeon, South Korea, October 29–November 2, 2018*, edited by A. M. Shirokov and A. I. Mazur (Pacific National

University, Khabarovsk, Russia, 2019), p. 310, http://ntse.khb.ru/files/uploads/2018/proceedings/Epelbaum.pdf.

[24] S. Kölling, E. Epelbaum, H. Krebs, and U.-G. Meißner, Phys. Rev. C **84**, 054008 (2011).

[25] H. Krebs, E. Epelbaum, and U.-G. Meißner, Few-Body Syst. **60**, 31 (2019).

[26] H. Krebs, Eur. Phys. J. A **56**, 234 (2020).

[27] O. Pisanti, A. Cirillo, S. Esposito, F. Iocco, G. Mangano, G. Miele, and P. D. Serpico, Comput. Phys. Commun. **178**, 956 (2008).

[28] R. J. Cooke, M. Pettini, and C. C. Steidel, Astrophys. J. **855**, 102 (2018).

[29] A. E. Cox, S. A. R. Wynchank, and C. H. Collie, Nucl. Phys. **74**, 497 (1965).

[30] D. Cokinos and E. Melkonian, Phys. Rev. C **15**, 1636 (1977).

[31] A. Tomyo, Y. Nagai, T. S. Suzuki, T. Kikuchi, T. Shima, T. Kii, and M. Igashira, Nucl. Phys. A **718**, 401 (2003).

[32] Y. Nagai, T. S. Suzuki, T. Kikuchi, T. Shima, T. Kii, H. Sato, and M. Igashira, Phys. Rev. C **56**, 3173 (1997).

[33] J. W. Chen and M. J. Savage, Phys. Rev. C **60**, 065205 (1999).

[34] G. Rupak, Nucl. Phys. A **678**, 405 (2000).

[35] S. R. Beane and M. J. Savage, Nucl. Phys. A **694**, 511 (2001).

[36] S. Ando, R. H. Cyburt, S. W. Hong, and C. H. Hyun, Phys. Rev. C **74**, 025809 (2006).

[37] S. R. Beane, E. Chang, W. Detmold, K. Orginos, A. Parreño, M. J. Savage, and B. C. Tiburzi (NPLQCD Collaboration), Phys. Rev. Lett. **115**, 132001 (2015).

[38] B. Acharya and S. Bacca, Phys. Lett. B **827**, 137011 (2022).

[39] H. Arenhovel and M. Sanzone, Few Body Syst. Suppl. **3**, 1 (1991).

[40] J. Carlson and R. Schiavilla, Rev. Mod. Phys. **70**, 743 (1998).

[41] L. E. Marcucci, K. M. Nollett, R. Schiavilla, and R. B. Wiringa, Nucl. Phys. A **777**, 111 (2006).

[42] B. R. Barrett, P. Navrátil, and J. P. Vary, Prog. Part. Nucl. Phys. **69**, 131 (2013).

[43] P. Navratil, J. P. Vary, and B. R. Barrett, Phys. Rev. C **62**, 054311 (2000).

[44] P. Navratil, J. P. Vary, and B. R. Barrett, Phys. Rev. Lett. **84**, 5728 (2000).

[45] S. Quaglioni and P. Navratil, Phys. Rev. Lett. **101**, 092501 (2008).

[46] S. Quaglioni and P. Navratil, Phys. Rev. C **79**, 044606 (2009).

[47] P. Navratil, S. Quaglioni, I. Stetcu, and B. R. Barrett, J. Phys. G: Nucl. Part. Phys. **36**, 083101 (2009).

[48] P. Navratil and S. Quaglioni, Phys. Rev. Lett. **108**, 042503 (2012).

[49] S. Baroni, P. Navratil, and S. Quaglioni, Phys. Rev. Lett. **110**, 022505 (2013).

[50] S. Baroni, P. Navratil, and S. Quaglioni, Phys. Rev. C **87**, 034326 (2013).

[51] S. Quaglioni, G. Hupin, A. Calci, P. Navratil, and R. Roth, EPJ Web Conf. **113**, 01005 (2016).

[52] J. Dohet-Eraly, P. Navrátil, S. Quaglioni, W. Horiuchi, G. Hupin, and F. Raimondi, Phys. Lett. B **757**, 430 (2016).

[53] P. Navrátil, S. Quaglioni, G. Hupin, C. Romero-Redondo, and A. Calci, Phys. Scr. **91**, 053002 (2016).

[54] G. Hupin, S. Quaglioni, and P. Navrátil, Nat. Commun. **10**, 351 (2019).

[55] K. Kravvaris, P. Navrátil, S. Quaglioni, C. Hebborn, and G. Hupin, arXiv:2202.11759.

[56] C. Hebborn, G. Hupin, K. Kravvaris, S. Quaglioni, P. Navrátil, and P. Gysbers, Phys. Rev. Lett. **129**, 042503 (2022).

[57] P. Navratil and S. Quaglioni, arXiv:2204.01187.

[58] A. M. Shirokov, A. I. Mazur, I. A. Mazur, and J. P. Vary, Phys. Rev. C **94**, 064320 (2016); **98**, 039901(E) (2018).

[59] A. M. Shirokov, G. Papadimitriou, A. I. Mazur, I. A. Mazur, R. Roth, and J. P. Vary, Phys. Rev. Lett. **117**, 182502 (2016); **121**, 099901(E) (2018).

[60] L. D. Blokhintsev, A. I. Mazur, I. A. Mazur, D. A. Savin, and A. M. Shirokov, Phys. At. Nucl. **80**, 1093 (2017).

[61] L. D. Blokhintsev, A. I. Mazur, I. A. Mazur, D. A. Savin, and A. M. Shirokov, Phys. At. Nucl. **80**, 226 (2017).

[62] A. M. Shirokov, A. I. Mazur, I. A. Mazur, E. A. Mazur, I. J. Shin, Y. Kim, L. D. Blokhintsev, and J. P. Vary, Phys. Rev. C **98**, 044624 (2018).

[63] A. I. Mazur, A. M. Shirokov, I. A. Mazur, L. D. Blokhintsev, Y. Kim, I. J. Shin, and J. P. Vary, Phys. At. Nucl. **82**, 537 (2019).

[64] J. M. Bang, A. I. Mazur, A. M. Shirokov, Y. F. Smirnov, and S. A. Zaytsev, Ann. Phys. **280**, 299 (2000).

[65] J. M. Blatt and V. F. Weisskopf, *Theoretical Nuclear Physics* (Dover, Mineola, NY, 2010).

[66] J. Suhonen, *From Nucleons to Nucleus: Concepts of Microscopic Nuclear Theory* (Springer, Berlin, 2007).

[67] G. B. Arfken, H. J. Weber, and F. E. Harris, *Mathematical Methods for Physicists: A Comprehensive Guide*, 7th ed. (Academic, New York, 2011).

[68] H. A. Yamani and L. J. Fishman, J. Math. Phys. **16**, 410 (1975).

[69] S. A. Zaitsev, Y. F. Smirnov, and A. M. Shirokov, Teor. Mat. Fiz. **117**, 227 (1998); S. A. Zaitsev, Y. F. Smirnov, and A. M. Shirokov, Theor. Math. Phys. **117**, 1291 (1998).

[70] A. M. Shirokov, A. I. Mazur, S. A. Zaytsev, J. P. Vary, and T. A. Weber, Phys. Rev. C **70**, 044005 (2004).

[71] B. Gyarmati, A. T. Kruppa, and J. Révai, Nucl. Phys. A **326**, 119 (1979).

[72] J. Revai, M. Sotona, and J. Zofka, J. Phys. G **11**, 745 (1985).

[73] A. Bohr and B. R. Mottelson, *Nuclear Structure* (World Scientific, Singapore, 1998).

[74] P. Maris, M. A. Caprio, and J. P. Vary, Phys. Rev. C **91**, 014310 (2015).

[75] S. Pal *et al.* (unpublished).

[76] S. Pal, Electroweak multipole operators from chiral effective field theory, Ph.D. thesis, Iowa State University, 2022 (unpublished).

[77] E. Epelbaum (private communication).

[78] C. Van Der Leun and C. Alderliesten, Nucl. Phys. A **380**, 261 (1982).

[79] A. Huber, T. Udem, B. Gross, J. Reichert, M. Kourogi, K. Pachucki, M. Weitz, and T. W. Hansch, Phys. Rev. Lett. **80**, 468 (1998).

[80] P. J. Mohr, D. B. Newell, and B. N. Taylor, Rev. Mod. Phys. **88**, 035009 (2016).

[81] R. V. Reid, Jr., and M. L. Vaida, Phys. Rev. Lett. **29**, 494 (1972); **34**, 1064 (1975).

[82] D. M. Bishop and L. M. Cheung, Phys. Rev. A **20**, 381 (1979).

[83] R. B. Wiringa, V. G. J. Stoks, and R. Schiavilla, Phys. Rev. C **51**, 38 (1995).

[84] J. A. Melendez, R. J. Furnstahl, D. R. Phillips, M. T. Pratola, and S. Wesolowski, Phys. Rev. C **100**, 044001 (2019).

[85] P. Reinert, H. Krebs, and E. Epelbaum, Eur. Phys. J. A **54**, 86 (2018).

[86] B. Acharya and S. Bacca, Phys. Rev. C **101**, 015505 (2020).

[87] B. Acharya, V. Lensky, S. Bacca, M. Gorchtein, and M. Vanderhaeghen, Phys. Rev. C **103**, 024001 (2021).